Gold Nanoparticles on Mesoporous Interparticle Networks of Titanium Dioxide Nanocrystals for Enhanced Photonic Efficiencies

ARTICLE *in* THE JOURNAL OF PHYSICAL CHEMISTRY C · APRIL 2009

Impact Factor: 4.77 · DOI: 10.1021/jp900766g

4 AUTHORS, INCLUDING:

Adel A Ismail
Central Metallurgical Research and Develo…
64 PUBLICATIONS **1,556** CITATIONS
SEE PROFILE

Michael Wark
Carl von Ossietzky University Oldenburg, G…
189 PUBLICATIONS **2,748** CITATIONS
SEE PROFILE

Article

Gold Nanoparticles on Mesoporous Interparticle Networks of Titanium Dioxide Nanocrystals for Enhanced Photonic Efficiencies

Adel A. Ismail, Detlef W. Bahnemann, Inga Bannat, and Michael Wark

J. Phys. Chem. C, **2009**, 113 (17), 7429-7435• Publication Date (Web): 03 April 2009

Gold Nanoparticles on Mesoporous Interparticle Networks of Titanium Dioxide Nanocrystals for Enhanced Photonic Efficiencies

Adel A. Ismail,*,† Detlef W. Bahnemann,† Inga Bannat,‡ and Michael Wark‡

Institut für Technische Chemie & Zentrum für Festkörperchemie and neue Materialien (ZFM), Leibniz Universität Hannover, Callinstrasse 3, D-30167 Hannover, Germany, and Institut für Physikalische Chemie and Elektrochemie & Zentrum für Festkörperchemie and neue Materialien (ZFM), Leibniz Universität Hannover, Callinstrasse 3-3a, 30167 Hannover, Germany

Received: January 26, 2009; Revised Manuscript Received: February 27, 2009

Nanocomposites consisting of Au and TiO_2 nanocrystals have been synthesized through simple one-step sol−gel reactions of titanium tetraisopropoxide with hydrogen tetrachloroaurate in the presence of an F127 triblock copolymer as the template to direct the formation of nanostructured photocatalysts. The thus formed Au/TiO_2 network gels were calcined at 500 °C for 4 h, leading to Au/TiO_2 nanocomposites with high interparticle mesoporosity, pore diameters of around 10 nm, and BET surface areas of about 100 m^2/g. TEM investigations of 0.5 wt % Au/TiO_2 reveal that the TiO_2 particles are quite uniform in size and shape. The particle sizes of TiO_2 and Au are in the range of 5−10 and 20−120 nm, respectively. The photocatalytic methanol oxidation to formaldehyde chosen as the test reaction to examine the photocatalytic activity of the Au/TiO_2 was shown to be more effective as compared with pure TiO_2 and with Degussa P25, respectively. The increased photocatalytic activity of Au/TiO_2 with interparticle mesopores is attributed to a higher intrinsic activity of the Au/TiO_2 and improved intrinsic electron diffusion. The latter effect is explained by considering the mesoporous TiO_2 network to behave like an antenna system for the photogenerated electrons, enabling them to reach the respective TiO_2/Au contacts with high probability. Thus, a few Au particles in electronic contact with the entire TiO_2 structure are sufficient to act as efficient electron relays, enabling the charge transfer to the solutes. The sample 0.5 wt % Au/TiO_2 nanocrystals with smaller Au nanoparticles is therefore more photoactive than those composed of larger Au particles and hence less semiconductor/metal contacts.

Introduction

Semiconductors are key materials in modern optoelectronic and photoelectrochemical devices, and unique electronic states resulting from the quantum size effect and high dispersion with downsizing make them even more interesting from the perspective of both fundamental studies and potential applications.[1] Recently, the coupling of semiconductors with molecules and other solids on the nanoscale has been reported to improve the performance of various devices, including those tested in photocatalysis and solar energy conversion,[2−4] photoluminescence,[5] electrochromic applications, and biosensors.[6] Moreover, investigations on semiconductor−metal composites have revealed that the deposition of metals on semiconductor surfaces enhances the efficiency of photocatalytic redox processes.[7] Au/titania nanostructured materials are attractive for a variety of optoelectronic and photonic applications[8] and have therefore been widely employed for photocatalytic as well as for catalytic applications.[9,10]

The basic requirements for photoactive materials are high crystallinity and large surface area. At the nanometer scale, the photocatalytic characteristics of a given material can be greatly enhanced by an increased surface area of the particles.[11] The effectiveness of titania as a photocatalyst depends on its crystal phase, particle size, surface area, and crystallinity.[12] Among the common crystalline forms of titania, anatase is generally recognized to be the most active phase. With regard to particle size, smaller particles are usually better photocatalysts due to their high surface area-to-volume ratio.[13] Once TiO_2 particles, however, reach the quantum size regime, i.e., diameter ≤3 nm, the widening of the optical band gap limits the usable photon energies. Clearly, an optimum particle size should exist, balancing the appropriate bandgap with a high surface area needed for adsorption of molecules.

Haruta et al. demonstrated that gold nanoparticles with 2−5 nm diameter show unusually high catalytic activities.[14] Similarly, Goodman et al. have demonstrated the influence of gold nanoparticle deposition on the overall catalytic activity of titania.[15] However, the influence of Au nanoparticle additives on the degree of crystallinity of the TiO_2 or the electron transport paths in the composites both determining the photocatalytic activity are much less understood.[16,17]

As a photocatalytic test reaction, the photooxidation of methanol to formaldehyde by $^{\bullet}OH$ attack is well established and investigated for powdered TiO_2,[18] TiO_2 (Evonik-Degussa) P25, Sachtleben Hombikat UV 100, and colloidal TiO_2[19] as well as 20% TiO_2/SiO_2 and TiO_2/SBA-15.[20] The efficiency of this photooxidation reaction very much depends on the photonic efficiency for the generation of $^{\bullet}OH$ radicals. Thus, an experimental method for the detection of the quantity of photons absorbed by aqueous TiO_2 dispersions was developed.[21] Among the pure TiO_2 phases, P25 (Evonik-Degussa) was found to exhibit the highest activity, but by using Fe_2O_3−TiO_2[22] and Pt@TiO_2[23] for the same reaction, the photonic efficiencies could be enhanced by a factor of 2.

* E-mail: a-ismail@iftc.uni-hannover.de.
† Institut für Technische Chemie & Zentrum für Festkörperchemie and neue Materialien (ZFM).
‡ Institut für Physikalische Chemie and Elektrochemie & Zentrum für Festkörperchemie and neue Materialien (ZFM).

10.1021/jp900766g CCC: $40.75
Published on Web 04/03/2009

TABLE 1: Physicochemical Properties of Pure TiO_2 and of Au/TiO_2 Nanoparticles Prepared with Different Au Contents and Their Photocatalytic Properties (Initial Reaction Rates and Photonic Efficiencies of 30 mM Methanol Photooxidation)[a]

photocatalyst	S_{BET} (m^2 g^{-1})	particle size (nm)	E_g (eV)	$r \times 10^7$ (mol^{-1} s^{-1})	ξ (%)	V_p (cm^3/g)	D_p (nm)
pure TiO_2	185.7	3.6	3.02	2.6	5.2	0.291	11.2
0.3 wt % Au/TiO_2	129.3	4.6	3.16	3.1	6.2	0.267	11.0
0.5 wt % Au/TiO_2	107.8	5.0	3.22	5.1	10.2	0.259	10.8
1 wt % Au/TiO_2	98.4	6.3	3.26	4.0	8.1	0.233	9.6
3 wt % Au/TiO_2	96.6	8.1	3.05	3.6	7.3	0.211	9.6
5 wt % Au/TiO_2	90.8	9.4	3.06	3.3	6.6	0.189	9.1
TiO_2 Degussa	50.0		3.20	2.1	4.2		

[a] S_{BET}, surface area; r, HCHO production rate; ξ, photonic efficiency; V_p, pore volume; D_p, pore diameter.

In this contribution, the photocatalytic efficiencies of mesoporous Au/TiO_2 networks for the photooxidation of methanol have been investigated. We report a simple yet general method to introduce nanoscale dispersions of gold particles into nanocrystalline TiO_2 networks with interparticle mesopores, and explain the relation of particle size, surface area, and particle arrangement with the photonic efficiencies for the first time. The increased photocatalytic activity of Au/TiO_2 with interparticle mesopores is attributed to a higher intrinsic activity of the Au/TiO_2 and improved intrinsic electron diffusion within an antenna-like network.

Experimental Section

Titania and Au/Titania Syntheses. The block copolymer surfactant $EO_{106}-PO_{70}EO_{106}$ (F127, EO = $-CH_2CH_2O-$, PO = $-CH_2(CH_3)CHO-$) was obtained from Sigma and titanium tetraisopropoxide, $Ti[OCH(CH_3)_2]_4$ (TTIP), methanol, and hydrogen tetrachloroaurate tetrahydrate ($HAuCl_4 \cdot 4H_2O$) were purchased from Aldrich and were used without further purification. Pure TiO_2 and Au/TiO_2 nanocrystals were synthesized through a simple one-step sol−gel process in the presence of the F127 triblock copolymer as a structure directing agent. To embed gold nanoparticles homogenously within the titania framework, a multicomponent assembly approach was utilized, where the surfactant, titania, and gold were assembled in an one-step process. Pure TiO_2 and Au/TiO_2 were prepared as follows: at first, 1.29 g of the triblock copolymer F127 was dissolved in 11 g of methanol by stirring for 30 min. Then, a solution of 9.84 g of TTIP in 1.44 mL of HCl (37%) was added under vigorous stirring for 10 min, followed by the dropwise addition of an aqueous solution (x mL) containing $HAuCl_4$ (1 mL = 0.04 g $HAuCl_4$) with further stirring for 10 min; x = 0.39, 0.64, 1.3, 2.59, 3.87, and 6.45 correspond to 0.3, 0.5, 1, 3, and 5 wt % Au in the Au/TiO_2 composites, respectively. To minimize possible variables, the molar ratio of each reagent in the starting solution was fixed at TiO_2/F127/HCl/H_2O/CH_3OH = 1:0.003:1:4:10. Finally, the sol was gelled at 40 °C in air for 30 min. By using TTIP instead of $TiCl_4$,[24] the gelation time was significantly reduced, from 7 days to 30 min. The gel samples were calcined at 500 °C for 4 h with a heating rate of 2 °C/min and a cooling rate of 2 °C/min in air to remove the surfactant and to obtain nanocrystalline Au/TiO_2 photocatalysts with interparticle mesopores.

Characterization. Wide-angle XRD (WXRD) data were acquired on a Bruker AXS D4 Endeavor X diffractometer using Cu $K\alpha_{1/2}$, $\lambda\alpha_1$ = 154.060 pm, $\lambda\alpha_2$ = 154.439 pm radiation. The nitrogen adsorption and desorption isotherms at 77 K were measured using a Quantachrome Autosorb 3B after vacuum-drying the samples at 200 °C overnight. The sorption data were analyzed using the Barrett−Joyner−Halenda (BJH) model with the Halsey equation.[25] The thermogravimetric analysis of the Au/TiO_2 gel was carried out at a heating rate of 10 °C/min from 20 to 1000 °C in flowing air (Setaram, Setsys Evolution-1750). FT-IR spectra were recorded with a BRUKER FRA 106 spectrometer using the standard KBr pellet method. TEM measurements were conducted at 200 kV with a JEOL JEM-2100F-UHR field-emission instrument equipped with a Gatan GIF 2001 energy filter and a 1k-CCD camera in order to obtain EEL spectra. SEM measurements were performed on a JEOL JSM-6700F field-emission instrument using a secondary electron detector (SE) at an accelerating voltage of 2 kV. The bandgap energy of the catalysts was determined using diffuse reflectance spectroscopy (DRS). The reflectance spectra of the samples over a range of 200−700 nm were recorded with a Varian Cary 100 Scan UV−vis system equipped with a Labsphere integrating sphere diffuse reflectance accessory and using $BaSO_4$ as a reference material.[26] A given amount of Au/TiO_2 powder was uniformly pressed in the sample holder that was placed at the integrating sphere for the reflectance measurements. The reflectance data was converted to the absorption coefficient $F(R)$ values according to the Kubelka−Munk equation.[27] The modified Kubelka−Munk function was determined using the equation as follows:

$$F(R) = \left(\frac{(1-R)^2}{2R} \times h\nu\right)^{1/2}$$

where R is the proportion of light reflected, h is Planck's constant, and ν is the frequency of light. Plots of this parameter were used to determine the bandgap energy from the linear portion of the absorption transition using least-squares regression and extrapolating to zero at the corresponding photon energy. The bandgap energies of catalysts were calculated according to the equation $E_g = hc/\lambda$, where E_g is the bandgap energy (eV), c the light velocity (m/s), and λ the wavelength (nm).

Photocatalytic Activity Tests. The photoreactor consisted of a quartz reactor with an effective volume of 75 mL, and UV irradiation was performed by a 450 W medium pressure xenon lamp (Osram) placed inside a quartz jacket and equipped with a cooling tube. The lamp was switched on 30 min before the beginning of the reaction to stabilize the power of its emission spectrum line $\lambda > 320$ nm (a cutoff filter was used to remove light with wavelengths below 320 nm), and the reactor was cooled by the circulation of H_2O. Reactions were carried out suspending 0.75 g/L of the Au/TiO_2 photocatalysts and purging oxygen through the reaction vessel continuously. The suspensions were sonicated at the desired concentration before the experiment was started. Samples were withdrawn at regular intervals from the upper part of the reactor with the catalyst being removed from the liquid phase by filtration through nylon syringe filters (pore size 0.22 μm). The photooxidation rate was determined by measuring the formaldehyde production employing the Nash method.[28] This method is based on the reaction of

SCHEME 1: Schematic Illustration of the Proposed Antenna Mechanism to Explain the Enhanced Activity for Methanol Photooxidation over Mesoporous Au/TiO_2 Nanocrystals As Photocatalysts

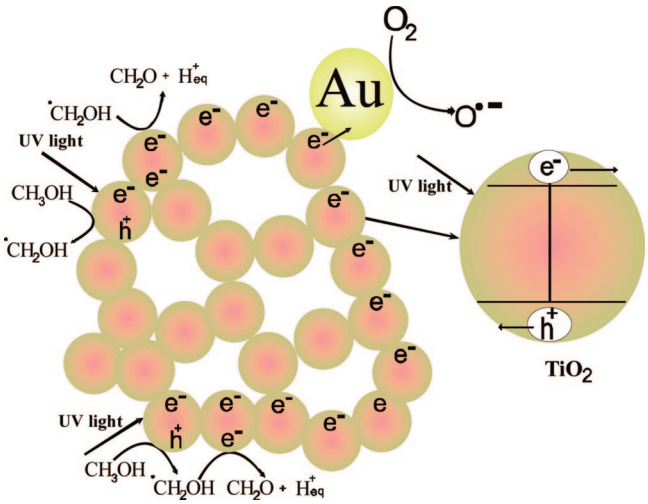

formaldehyde with acetylacetone and ammonium acetate to form a yellow colored product with a maximum of absorbance at 412 nm. Measurements were carried out using a Varian Cary 100 Scan UV−vis spectrophotometer, following an incubation time of 15 min at 60 °C. The photonic efficiency was calculated for each experiment as the ratio of the photocatalytic oxidation rate and the incident light intensity, as given in the following equation.[29]

$$\xi = \frac{r \times 100}{I}$$

where ξ is the photonic efficiency (%), r the photooxidation rate of methanol (mol L^{-1} s^{-1}), and I the incident photon flux (4.94×10^{-6} E L^{-1} s^{-1}). The UV-A incident photon flow was determined by ferrioxalate actinometry.[19]

Results and Discussion

Structural Investigations. Nanocrystalline networks TiO_2 and Au/TiO_2 were synthesized through a simple one-step sol−gel process in the presence of a F127 triblock copolymer as a structure directing agent. The use of surfactants enables the controlled synthesis of uniform TiO_2 nanocrystals with very small particle size (about 5 nm) in one step. High uniformity in size and shape is essential for achieving enhanced photocatalytic activities (see Scheme 1). By using methanol[24] as the solvent, the photocatalytically more active TiO_2 phase anatase is exclusively obtained. Because the thermodynamic stability is particle-size-dependent, at particle diameters <16 nm, anatase has been shown to be more stable than the rutile phase.[31] The Au/TiO_2 photocatalysts were prepared with various gold contents of 0, 0.3, 0.5, 1, 3, and 5 wt % Au/TiO_2 at a fixed F127:TTIP molar ratio of 0.003. The compositions and pore parameters of pure TiO_2 and Au/TiO_2 nanoparticles with interparticle mesopores are summarized in Table 1.

The X-ray diffraction (XRD) patterns in Figure 1 show Au/TiO_2 as-made and pure TiO_2 and Au/TiO_2 annealed at 500 °C for 4 h. The absence of any reflection reveals that the as-made sample is amorphous. Calcination at 500 °C initiated crystallization and the appearance of the (101), (004), (200), and (211) anatase peaks (powder diffraction file no. 86-1157, ICCD). At

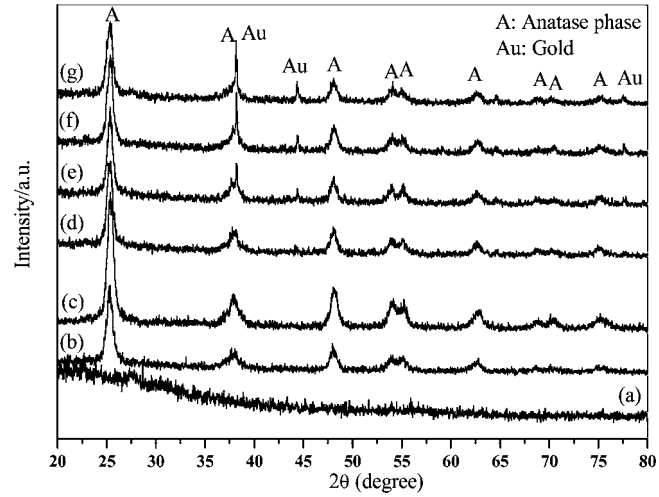

Figure 1. XRD patterns for the as-made 1 wt % Au/TiO_2 (a) and pure TiO_2 (b), 0.3 wt % Au/TiO_2 (c), 0.5 wt % Au/TiO_2 (d), 1 wt % Au/TiO_2 (e), 3 wt % Au/TiO_2 (f), 5 wt % Au/TiO_2 (g) nanocrystalline obtained from calcination at 500 °C for 4 h. Au(111) and (200) diffraction planes are recognizable in samples e−g, while anatase TiO_2 (101) and (200) lattice planes are detectable in all calcined samples.

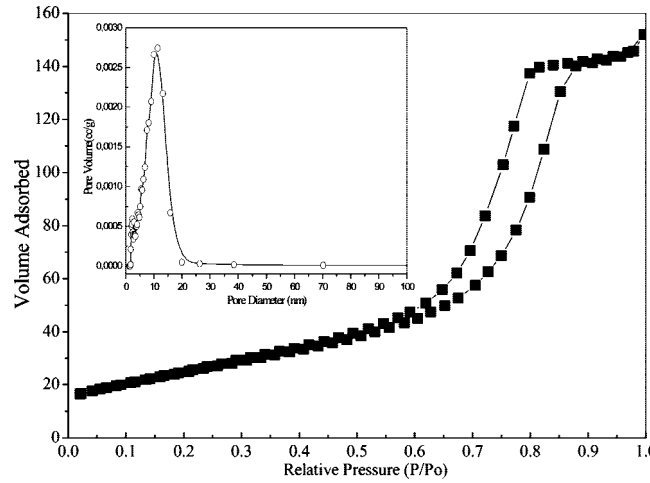

Figure 2. Nitrogen adsorption−desorption isotherms and BJH pore-size distribution plot (inset) for mesoporous 0.5 wt % Au/TiO_2 after calcinations at 500 °C for 4 h.

0.3 and 0.5 wt % Au/TiO_2, no crystalline phase involving gold can be observed, suggesting that either the gold is highly dispersed in the TiO_2 network or that the Au content is below the detection limit. On the other hand, at 1, 3, and 5 wt % Au/TiO_2, the cubic lattice of crystalline gold peaks was detected in the patterns from the (111) and (200) reflections (powder diffraction file no. 04-0784). The crystallinity and the particle size of the TiO_2 anatase phase were found to increase slightly with the Au content. The particle sizes given in Table 1 were estimated by applying Scherrer's equation[32] on the TiO_2 (101) reflection at $2\theta = 25.2°$ using the full width at half-maximum (fwhm).

In the N_2 adsorption/desorption studies, large hysteresis loops that resemble typical H_2-type isotherms are observed for 0.5 wt % Au/TiO_2 samples after calcination at 500 °C for 4 h (Figure 2). Such strong hysteresis is usually related to the capillary condensation associated with large mesopores. The Barrett−Joyner−Halenda (BJH) analysis shows that the 0.5 wt % Au/TiO_2 mesoporous network exhibits mean pore sizes of about 11 nm (Figure 2, inset) but also demonstrates that the pore-size distribution is quite wide. The BET surface area of this sample

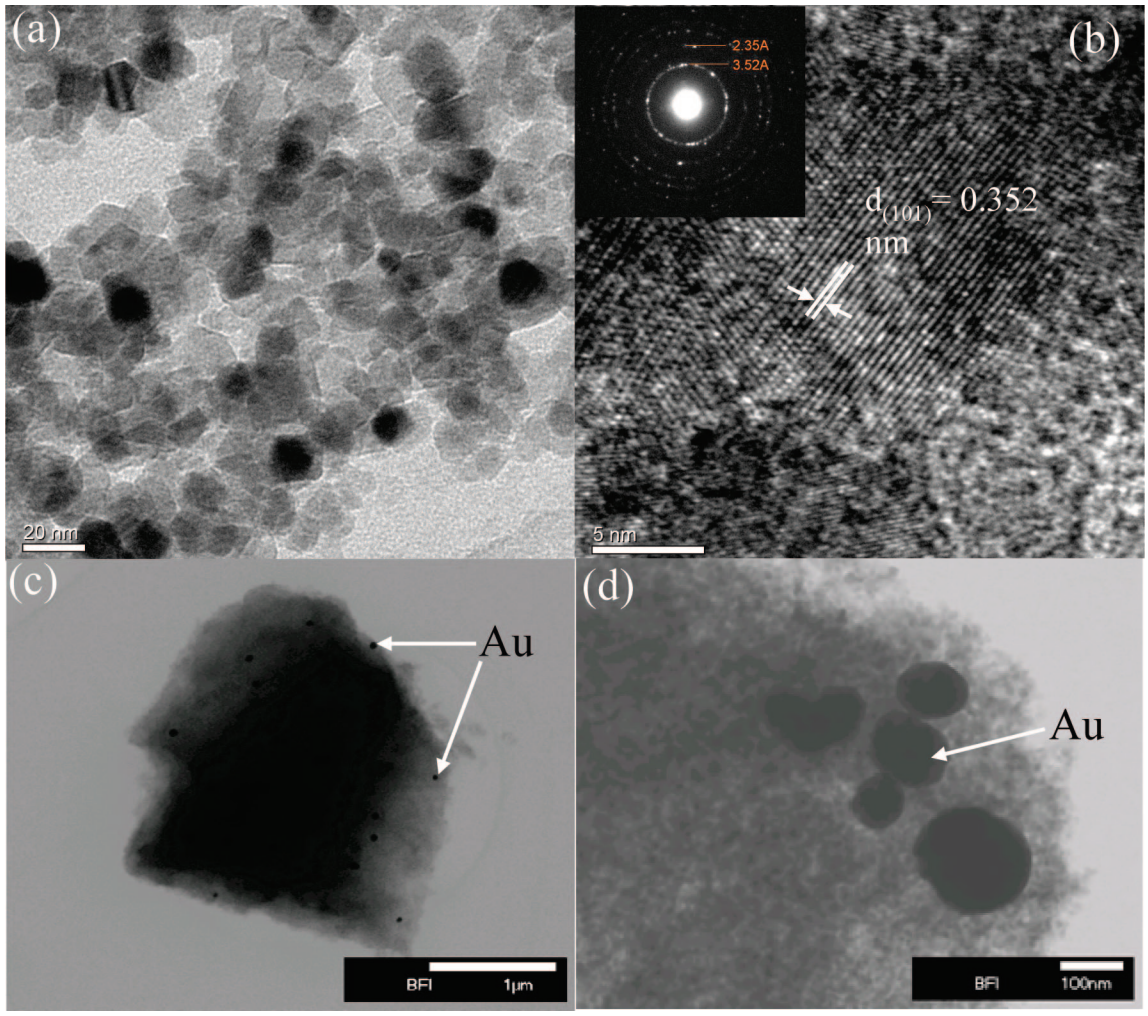

Figure 3. Representative TEM micrographs of a sample calcined at 500 °C for 4 h. (a) The overview proves the exclusive presence of 0.5 wt % Au/TiO_2 nanoparticles with an average diameter of about 5 nm; the particles are not agglomerated and quite uniform in size and shape. HRTEM image 0.5 wt % Au/TiO_2 nanoparticles (b) and selective area electron diffraction (SAED, inset b) and BF-TEM of 0.5 and 5 wt % Au/TiO_2 nanoparticles (c) and (d), respectively.

is 108 m^2/g; the BET surface areas, the pore volumes, and the pore diameters of all calcined TiO_2 and Au/TiO_2 samples are summarized in Table 1. With increasing gold loading, the surface areas decrease from 185 to about 90 m^2/g, reflecting the increase in size of the anatase nanoparticles. Surprisingly, the average pore size decreases only slightly from around 11 to about 9 nm, indicating that the size of the interparticle pores is mainly determined by the F127 block copolymer acting as a pore-filling template in the as-synthesized samples. The structural integrity of the formed TiO_2 and Au/TiO_2 networks is apparently retained during the F127 destruction by calcination at 500 °C, leading to a mesoporosity with pore sizes being to the best of our knowledge the largest ever reported for titania.

TEM images of the nanocrystalline 0.5 wt % Au/TiO_2 frameworks are presented in Figure 3. An overview image at low magnification illustrates that the product is almost exclusively composed of discrete Au/TiO_2 nanoparticles agglomerated into a mesoporous network (Figure 3a and Supporting Information Figure S1). Although it is rather difficult to observe the grain boundaries clearly, it can be said that the particles are quite uniform in size and shape (Figure 3a). Both the HRTEM image (Figure 3b) and the selective area electron diffraction (SAED, inset of Figure 3b) show well resolved (101) lattice fringes (distance 0.352 nm) and diffraction cycles indicative of a highly crystalline TiO_2 anatase framework. The Au nanoparticles can be more easily found in bright field TEM (BF-TEM) images (Figure 3c and d), showing that the average Au particle diameters increase from ~20 nm in the 0.5 wt % Au/TiO_2 sample to 50−120 nm for the samples with high Au content. The growth of the Au particles is also confirmed by the decrease of the XRD line width (Figure 1) with increasing Au content. Energy dispersive X-ray spectra (EDXS) also reveal the presence of Au (Supporting Information Figure S2) and confirm that the final Au content in the composite materials is consistent with the Au:Ti ratio used in the starting sol mixtures. In general, no mesostructure with long-range order is observed in the TEM images in good agreement with the fact that no peaks were observed in the small-angle X-ray diffraction (SXRD).

Figure 4 displays the TGA weight loss and the DTA of the as-made Au/TiO_2 gel (Figure 4). To replicate the calcination conditions outlined in the Experimental Section, the analysis was carried out at a heating rate of 10 °C/min from 20 to 1000 °C. These investigations reveal that, below 120 °C, 14.6% mass loss and a small endothermic peak are observed, representing the removal of volatile species (methanol and H_2O). Between 120 and 280 °C, a mass loss of 36.5% arises and an exothermic peak appears, corresponding to the oxidation of the F127 template. Some residual organic matter, such as amorphous carbon and possibly hydroxyl groups, was removed at 280−380 °C corresponding to a mass loss of ~10% (Figure 4).[33]

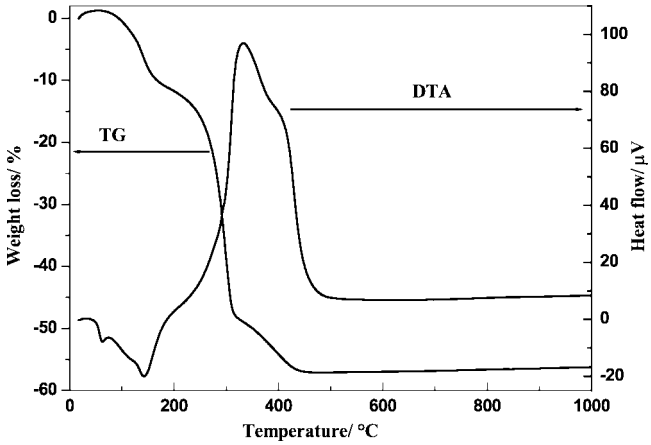

Figure 4. TG weight loss and DTA of 1 wt % Au/TiO_2 gel.

The exothermic peak at approximately 425 °C most likely can be attributed to the amorphous-to-anatase phase transition in TiO_2.

The removal of the F127 template by calcination at 500 °C for 4 h is also demonstrated by FTIR measurements showing the disappearance of the νCH bands around 2875 cm^{-1} as well as of the bands at 1115, 1242, 1297, 1378, and 1460 cm^{-1} originating from interactions of the $HAuCl_4$ with the block copolymer (Supporting Information Figure S3). The remaining broad peak ranging from 3250 to 3630 cm^{-1} can be attributed to OH species and surface-adsorbed H_2O; the absorption peaks around 1640 cm^{-1} are attributed to the vibrations of the surface-adsorbed H_2O and Ti−OH bonds. In general, calcination at 500 °C removes the template and decomposes Ti−O−Au bonds, creating nanocrystalline TiO_2 and Au nanoparticles.[9a]

The bandgap energy of the Au/TiO_2 nanoparticles (determined from the optical measurements) ranges between 3.05 and 3.22 eV, and thus does not differ from that of pure TiO_2 (3.02 eV, cf. Table 1 and Supporting Information Figure S4). Because even the smallest anatase particles in the pure TiO_2 sample exhibit bulk behavior and do not show any size quantization, the slight observed increase in particle size has no influence on the bandgap energy. Also, the presence of Au does not alter the TiO_2 absorption spectrum.

Photocatalytic Oxidation of Methanol. When photons with energies >3.2 eV, i.e., exceeding the band gap energy of TiO_2, are absorbed by the anatase particles in the mesoporous Au/TiO_2 photocatalysts, electrons are rapidly promoted from the valence band to the conduction band, leaving holes behind in the valence band (Scheme 1). The thus formed electrons and holes participate in redox processes at the semiconductor/water interface. The valence band holes migrate to the surface of the particles where they react with adsorbed hydroxide ions (or water molecules), generating adsorbed $^{\bullet}OH$ radicals. At the same time, the conduction band electrons migrate through the three-dimensional TiO_2 network until they reach a Au nanoparticle where adsorbed molecular oxygen is reduced to form $O_2^{\bullet-}$ radicals (eq 4). The α-hydroxy methyl radicals, formed from the reaction of the adsorbed $^{\bullet}OH$ radicals with the adsorbed methanol molecules can react with oxygen to form further $HO_2^{\bullet}$ radicals (eq 5). Alternatively, they can transfer an additional electron to the conduction band of the mesoporous TiO_2 network which is accompanied with the formation of a proton (see Scheme 1 and eqs 1−8[1b,19,20]). This latter process corresponds to the so-called current doubling effect (eqs 1, 5, and 6).

$$TiO_2 + h\nu \rightarrow TiO_2(e_{cb}^- + h_{vb}^+) \quad (1)$$

$$h_{vb}^+ + OH_s^- \rightarrow {}^{\bullet}OH_s \quad (2)$$

$$TiO_2(e_{cb}^-) + Au \rightarrow TiO_2{-}Au(e^-) \quad (3)$$

$$TiO_2{-}Au(e^-) + O_2 \rightarrow TiO_2{-}Au + O_2^{-\bullet} \quad (4)$$

$$CH_3OH + {}^{\bullet}OH_s \rightarrow {}^{\bullet}CH_2OH + H_2O \quad (5)$$

$${}^{\bullet}CH_2OH + TiO_2 \rightarrow HCHO + TiO_2(e^-) + H_{aq}^+ \quad (6)$$

$${}^{\bullet}CH_2OH + O_2 \rightarrow HCHO + HO_2^{\bullet} \quad (7)$$

$$2e^- + O_2 + 2H_{eq}^+ \rightarrow H_2O_2 \quad (8)$$

The methanol photooxidation experiments performed here showed no reaction under UV illumination in the absence of the synthesized Au/TiO_2 nanocomposites and also when the Au/TiO_2 samples were in contact with methanol in the dark. The data obtained during the illumination of the Au/TiO_2 nanocomposites with UV light are shown in Figure 5 and summarized in Table 1. They reveal that the photonic efficiency increases with increasing Au content up to 0.5 wt % Au/TiO_2 with the maximum photonic efficiency being 10.2%. Subsequently, the photonic efficiency gradually decreases with increasing Au/Ti ratio, reaching a value of 6.6% for the sample containing 5 wt % Au. In addition, the Au/TiO_2 nanocomposites with interparticle mesopores are more photoactive than the commercially available photocatalyst powder P25 (Table 1 and Figure 5). Apparently, the Au particles serve as active sites for the electron transfer to O_2, on which the trapped photogenerated electrons are transferred to adsorbed molecular oxygen to produce $O_2^{\bullet-}$ radicals (eqs 3 and 4).

Typically, the photogenerated electrons will be distributed between the TiO_2 and the Au nanoparticles provided that they are in close contact.[1b] Migration of the photogenerated electrons from TiO_2 to Au occurs until the equilibration of quasi-Fermi level in the entire system is reached, while the double-layer charging around the metal nanoparticle facilitates the storage of the electrons on the gold nanoparticles.[36] Due to this electron accumulation the Quasi-Fermi level of Au increases to more negative potentials.[35] Such a shift in the Fermi level enhances the efficiency of the interfacial charge-transfer process in the composite system, and the resulting quasi-Fermi level shifts closer to the conduction band of the semiconductor.[1b] In turn, it has been reported that smaller gold particles (interacting with charged TiO_2) and the loading amount induce more negative quasi-Fermi level shifts than bigger particles with the negative shift in the quasi-Fermi level indicating a better charge separation and thus a higher reductive power for the photocatalyst.[37] This is in good agreement with the observation of the present study that Au/TiO_2 nanocomposites with smaller gold nanoparticles (0.5 wt % Au/TiO_2) exhibit, in general, a higher photocatalytic activity than those with larger gold particles (≥1 wt % Au/TiO_2). Similar results concerning the size-dependent catalytic properties of gold nanoparticles deposited on titania have been obtained in earlier studies.[14b]

In addition, the increased photocatalytic activity of Au/TiO_2 nanocrystals with interparticle mesopores can be attributed to

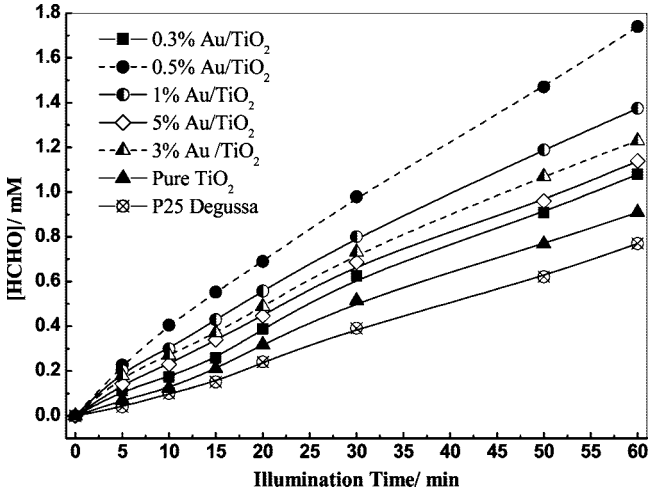

Figure 5. Photooxidation of methanol over pure TiO_2 and Au/TiO_2 nanocrystalline and Degussa P25 photocatalysts for HCHO production as a function of illumination time. Photocatalyst loading, 0.75 g/L; 30 mM aqueous CH_3OH (O_2^- saturated, natural pH; $T = 20$ °C); reaction volume, 75 mL; $I_o = 4.49 \times 10^{-6}$ Einstein L^{-1} s^{-1} (ca. >320 nm).

a higher intrinsic activity of the photocatalyst, enabling high flux and rapid methanol diffusion, thus increasing the photonic efficiency. Therefore, the highest activity observed for the 0.5 wt % Au/TiO_2 nanocomposites can be ascribed to the most efficient charge separation through the interparticle pore charge transfer.[38]

On the other hand, it is interesting to analyze the geometric parameters of the employed Au/TiO_2 systems in more detail. Assuming a spherical geometry of the particles, the volume of one Au nanoparticle (the particle diameter is 20 nm for 0.5 wt % Au/TiO_2) is 4189 nm^3. Taking the density of gold (19.3 g cm^{-3}), the average weight of one Au nanoparticle is calculated to be 8.08×10^{-17} g. Likewise, the average weight of one 5 nm TiO_2 nanoparticle (3.894 g cm^{-3}) is 2.55×10^{-19} g. Therefore, the molar ratio between Au and TiO_2 nanoparticles for the 0.5 wt % Au/TiO_2 preparation is calculated to be about 1:60 000. For the 5 wt % Au/TiO_2 samples (with larger Au particles of 120 nm diameter in average), the molar ratio of Au and TiO_2 is calculated to be about 1:200 000.

At first glance, it is therefore surprising that Au promotes the photocatalytic oxidation of methanol to formaldehyde that effectively, although this rough calculation as well as the TEM images show that rather large Au particles are present and that only very few anatase nanoparticles are in direct contact with an Au particle (Figure 3c,d). Clearly, the observed increase in photocatalytic efficiency cannot simply be explained by assuming that the entire mesoporous network behaves like a single crystal with porous structure, since such an assumption would be applicable also to other Au/TiO_2 systems which, however, do not exhibit such an increase in photocatalytic efficiency.[39] As an alternative mechanism it is therefore suggested that the so-called antenna mechanism[40] can be employed to explain the efficient photooxidation of methanol using the Au/TiO_2 mesopores. Thus, the three-dimensional mesoporous TiO_2 network acts as an antenna system transferring the initially generated electrons from the location of light absorption to a suitable interface with the noble metal catalyst and subsequently to the location of the Au nanoparticle where the actual electron-transfer reaction will take place.[40] This mechanism is schematically presented in Scheme 1. While earlier studies concerning the antenna effect in photocatalysis have been performed employing self-aggregated nanoparticulate systems, the presently studied material has been specially designed as a mesoporous network of nanoparticles. Within this antenna model, it can be envisaged that the overlap of the energy bands of the nanoparticles forming this network will result in unified energy bands for the entire system, enabling a quasi-free movement of the photogenerated charge carriers throughout. Consequently, an electron generated by light absorption within one of the nanoparticles forming the network will subsequently be available to promote redox processes anywhere within the structure. Upon the basis of the energetic considerations discussed above (quasi-Fermi level concept), the energetically most favored location for this electron should be the contact of the mesoporous TiO_2 structure with the Au nanoparticle, resulting in the enhanced photocatalytic activity of Au/TiO_2 reported here.

Assuming a Schottky contact between the mesoporous titanium dioxide network and the noble metal particle, the Au particles then serve as active sites for the reduction of molecular oxygen, on which the trapped photogenerated electrons are transferred to oxygen producing $O_2^{\bullet -}$ radicals. It should be noted that it is frequently overseen that this latter process is really the "bottleneck" in most photocatalytic transformations, being the rate-determining step due to its very small thermodynamic driving force. Thus, its acceleration through the electron-transfer catalysis induced by the Au deposits will result in the observed increase in the yield of the photocatalytic methanol oxidation.

Summary and Conclusions

This study illustrates the successful synthesis of pure TiO_2 and Au/TiO_2 nanocomposites with interparticle mesopores via a sol−gel route. The formed anatase particles are only slightly agglomerated and quite uniform in size and shape. With interparticle pore diameters of up to 11 nm, the pores formed in these Au/TiO_2 networks using this procedure and resulting from a subsequent controlled calcination step are the largest ever reported for mesoporous TiO_2. Photocatalytic results indicate that these Au/TiO_2 nanocomposites with interparticle mesoporosity enable high flux and rapid diffusion of methanol. The newly prepared Au/TiO_2 nanocrystals with interparticulate mesopores are thus highly efficient photocatalysts for the oxidation of methanol even though the calculated ratio of Au to TiO_2 particles is extremely small and considered to be unfavorable. The so-called antenna mechanism is proposed to explain these unexpected findings.

Acknowledgment. A.A.I. acknowledges the Alexander von Humboldt (AvH) Foundation for granting him a research fellowship. We thank Drs. A. Feldhoff and R. Marschall (Institute of Physical Chemistry and Electrochemistry, Leibniz University Hannover) for recording HRTEM images and for N_2 adsorption/desorption measurements and L. Robben and Prof. C.H. Rüscher (Institute of Mineralogy, Leibniz Universität Hannover) for XRD measurements and TG-DTA analysis.

Supporting Information Available: Representative TEM micrographs of 1 wt % Au/TiO_2; EDX analysis of 1 wt % Au/TiO_2; FTIR spectra for 1 wt % Au/TiO_2; UV−vis Kubelka−Munk transformed diffuse reflectance spectra for all samples. This material is available free of charge via the Internet at http://pubs.acs.org.

References and Notes

(1) (a) Tada, H.; Mitsui, T.; Kiyonaga, T.; Akita, T.; Tanaka, K. *Nat. Mater.* **2006**, *5*, 782. (b) Subramanian, V.; Wolf, E. E.; Kamat, P. V. *J. Am. Chem. Soc.* **2004**, *126*, 4943.

(2) Grätzel, M. Photoelectrochemical cells. *Nature (London)* **2001**, *414*, 338.
(3) Gur, I.; Fromer, N. A.; Geier, M. L.; Alivisatos, A. P. *Science* **2005**, *310*, 462.
(4) Li, G.; Li, L.; Boerio-Goates, J.; Woodfield, B. F. *J. Am. Chem. Soc.* **2005**, *127*, 8659.
(5) Ohko, Y.; Tatsuma, T.; Fujii, T.; Naoi, K.; Niwa, C.; Kubota, Y.; Fujishima, A. *Nat. Mater.* **2003**, *2*, 29.
(6) Xu, J.; Zhao, W.; Luo, X.; Chen, H. *Chem. Commun.* **2005**, 792.
(7) (a) Ikeda, S.; Sugiyama, N.; Pal, B.; Marci, G.; Palmisano, L.; Noguchi, H.; Uosaki, K.; Ohtani, B. *Phys. Chem. Chem. Phys.* **2001**, *3*, 267. (b) Dawson, A.; Kamat, P. V. *J. Phys. Chem. B* **2001**, *105*, 960. (c) Szabo-Bardos, E.; Czili, H.; Horvath, A. *J. Photochem. Photobiol., A* **2003**, *154*, 195.
(8) (a) Boettcher, S. W.; Fan, J.; Tsung, C.-K.; Shi, Q.; Stucky, G. D. *Acc. Chem. Res.* **2007**, *40*, 784. (b) Kiyonaga, T.; Mitsui, T.; Torikoshi, M.; Takekawa, M.; Soejima, T.; Tada, H. *J. Phys. Chem. B* **2006**, *110*, 10771–10778. (c) Pietron, J. J.; Stroud, R. M.; Rolison, D. R. *Nano Lett.* **2002**, *2*, 545.
(9) (a) Li, H.; Bian, Z.; Zhu, J.; Huo, Y.; Li, H.; Lu, Y. *J. Am. Chem. Soc.* **2007**, *129*, 4538. (b) Wua, G.; Chena, T.; Sua, W.; Zhoua, G.; Zonga, X.; Leia, Z.; Lia, C. *Int. J. Hydrogen Energy* **2008**, *33*, 1243. (c) Idakiev, V.; Tabakova, T.; Yuan, Z.-Y.; Su, B.-L. *Appl. Catal., A* **2004**, *270*, 135. (d) Yan, W.; Chen, B.; Mahurin, S. M.; Hagaman, E. W.; Dai, S.; Overbury, S. H. *J. Phys. Chem. B* **2004**, *108*, 2793.
(10) (a) Subramanian, V.; Wolf, E. E.; Kamat, P. V. *Langmuir* **2003**, *19*, 469. (b) Li, W.-C.; Comotti, M.; Schüth, F. *J. Catal.* **2006**, *237*, 190. (c) Dai, K.; Peng, T.; Chen, H.; Zhang, R.; Zhang, Y. *Environ. Sci. Technol.* **2008**, *42*, 1505. (d) Laberty-Robert, C.; Kuemmel, M.; Allouche, J.; Boissiere, C.; Nicole, L.; Grosso, D.; Sanchez, C. *J. Mater. Chem.* **2008**, *18*, 1216. (e) Li, J.; Zeng, H. C. *Chem. Mater.* **2006**, *18*, 4260.
(11) (a) Saadoun, L.; Ayllon, J. A.; Jimenez-Becerril, J.; Peral, J.; Domenech, X.; Rodrıguez-Clemente, R. *Appl. Catal., B* **1999**, *21*, 269. (b) Zheng, J.-Y.; Pang, J.-B.; Qiu, K.-Y.; Wei, Y. *J. Mater. Chem.* **2001**, *11*, 3367. (c) Zhang, Y.; Weidenkaff, A.; Reller, A. *Mater. Lett.* **2002**, *54*, 375.
(12) (a) Kondo, J. N.; Domen, K. *Chem. Mater.* **2008**, *20*, 835–847. (b) Li, J.; Yamada, Y.; Murakoshi, K.; Nakatoa, Y. *Chem. Commun.* **2001**, 2170. (c) Lin, H.; Huang, C. P.; Li, W.; Ni, C.; Shah, S. I.; Tseng, Y.-H. *Appl. Catal., B* **2006**, *68*, 1–11.
(13) Wang, Y.; Suna, A.; Mahler, W.; Kasowski, R. *J. Chem. Phys.* **1987**, *87*, 7315.
(14) (a) Bamwenda, G. R.; Tsubota, S.; Kobayashi, T.; Haruta, M. *J. Photochem. Photobiol., A* **1994**, *77*, 59. (b) Haruta, M. *Catal. Today* **1997**, *36*, 153.
(15) (a) Valden, M.; Lai, X.; Goodman, D. W. *Science* **1998**, *281*, 1647. (b) Yang, Z. X.; Wu, R. Q.; Goodman, D. W. *Phys. Rev. B* **2000**, *6*, 14066.
(16) (a) Lu, G. M.; Zhao, R.; Qian, G.; Qi, Y. X. *Catal. Lett.* **2004**, *97*, 115. (b) Sreethawong, T.; Yoshikawa, S. *Catal. Commun.* **2005**, *6*, 661.
(17) Wang, X. C.; Yu, J. C.; Ho, C.; Mak, A. C. *Chem. Commun.* **2005**, 2262.
(18) Sun, L.; Bolton, J. R. *J. Phys. Chem.* **1996**, *100*, 4127.
(19) (a) Wang, C.; Bahnemann, D. W.; Dohrmann, J. K. *Water Sci. Technol.* **2001**, *44*, 279–286. (b) Wang, C. Y.; Rabani, J.; Bahnemann, D. W.; Dohrmann, J. K. *J. Photochem. Photobiol., A* **2002**, *148*, 169–176. (c) Salinaro, A.; Emeline, A.; Zhao, J.; Hidaka, H.; Ryabchuk, V. K.; Serpone, N. *Pure Appl. Chem.* **1999**, *71*, 321–335. (d) Serpone, N.; Salinaro, A. *Pure Appl. Chem.* **1999**, *71*, 303–320.
(20) Marugan, J.; Hufschmidt, D.; Lopez-Munoz, M.-J; Selzer, V.; Bahnemann, D. W. *Appl. Catal., B* **2006**, *62*, 201–207.
(21) Schiavello, M.; Augugliaro, V.; Palmisano, L. *J. Catal.* **1991**, *127*, 332.
(22) (a) Wang, C. Y.; Bahnemann, D. W.; Dohrmann, J. K. *Chem. Commun.* **2000**, *153*, 9–1540. (b) Wang, C. Y.; Böttcher, C.; Bahnemann, D. W.; Dohrmann, J. K. *J. Mater. Chem.* **2003**, *13*, 2322.
(23) Wang, C.; Pagel, R.; Bahnemann, D. W.; Dohrmann, J. K. *J. Phys. Chem. B* **2004**, *108*, 14082–14092.
(24) Luo, H.; Wang, C.; Yan, Y. *Chem. Mater.* **2003**, *15*, 3841–3846.
(25) Gregg, S. J.; Sing, K. S. W. *Adsorption, surface area and porosity*; Academic Press: London, 1982.
(26) Grätzel, M. *Heterogeneous Photochemical Electron Transfer*; CRC Press: Baton Rouge, LA, 1988.
(27) Tauc, J.; Grigorovici, R.; Vanuc, A. *Phys. Status Solidi* **1966**, 15627.
(28) Nash, T. *Biochem. J.* **1953**, *55*, 416.
(29) Serpone, N.; Terzian, R.; Lawless, D.; Kennepohl, P.; Sauve, G. *J. Photochem. Photobiol., A* **1993**, *73*, 11.
(30) Zhang, H.; Banfield, J. F. *J. Mater. Chem.* **1998**, *8*, 2073.
(31) Zhang, H.; Banfield, J. F. *J. Phys. Chem. B* **2000**, *104*, 3481.
(32) Azároff, L. V.; Buerger, M. J. *The powder method in x-ray crystallography*; New York, 1958; p 255.
(33) (a) Choi, S. Y.; Mamak Coombs, M.; Chopra, N. N.; Ozin, G. A. *Adv. Funct. Mater.* **2004**, *14*, 335–344. (b) Alberius, P. A.; Frindell, K. L.; Hayward, R. C.; Kramer, E. J.; Stucky, G. D.; Chmelka, B. F. *Chem. Mater.* **2002**, *14*, 3284–3294.
(34) Li, H. X.; Li, J. X.; Huo, Y. N. *J. Phys. Chem. B* **2006**, *110*, 1559.
(35) (a) Wood, A.; Giersig, M.; Mulvaney, P. *J. Phys. Chem. B* **2001**, *105*, 8810. (b) Jakob, M.; Levanon, H.; Kamat, P. V. *Nano Lett.* **2003**, *3*, 353. (c) Subramanian, V.; Wolf, E. E.; Kamat, P. V. *J. Phys. Chem. B* **2003**, *107*, 7479.
(36) Chen, S.; Murray, R. W. *J. Phys. Chem. B* **1999**, *103*, 9996.
(37) Kiyonaga, T.; Fujii, M.; Akita, T.; Kobayashic, H.; Tada, H. *Phys. Chem. Chem. Phys.* **2008**, *10*, 6553.
(38) (a) Lakshminarasimhan, N.; Bae, E.; Choi, W. *J. Phys. Chem. C* **2007**, *111*, 15244. (b) Huang, Y.; Ho, W.; Lee, S.; Zhang, L.; Li, G.; Yu, J. C. *Langmuir* **2008**, *24*, 3510.
(39) Paramasivam, I.; Macak, J. M.; Schmuki, P. *Electrochem. Commun.* **2008**, *10*, 71.
(40) (a) Wang, C.-Y.; Pagel, R.; Dohrmann, J. K.; Bahnemann, D. W. *C. R. Chim.* **2006**, *9*, 761. (b) Friedmann, D.; Hansing, H.; Bahnemann, D. *Z. Phys. Chem.* **2007**, *221*, 329. (c) Lakshminarasimhan, N.; Kim, W.; Choi, W. *J. Phys. Chem. C* **2008**, *112*, 20451.

JP900766G